# Impact Loading Analysis of an Earthen Masonry Structure Using Finite Element Methods

Demiana Tse[1(✉)], João M. Pereira[2], and Paulo B. Lourenço[2]

[1] Wiss, Janney, Elstner Associates, Inc., 50 Congress Street, Suite 430, Boston, MA 02109, USA
dtse@wje.com

[2] ISISE, Department of Civil Engineering, University of Minho, 4800-058 Guimarães, Portugal

**Abstract.** Throughout the years, historical monuments have been at risk from natural and man-made causes. Impact loading analysis plays an important role in structural engineering and is one of the risks to existing construction, whether being through partial collapses, vehicle crashes, or historical or modern-day warfare. This case study analyses the local response of a wall portion of the Torre de la Vela, a rammed earth tower within the UNESCO World Heritage Site of the Alhambra, Grenada, under impact loading. For this case study, the wall section of the tower was modelled with finite element methods (FEM) using different modelling approaches: using a continuum model, using a continuum model with removal of damaged elements, and using a contact element model. The Concrete Damage Plasticity (CDP) material model was adopted for the rammed earth structure. Different impactors were considered, including a cannonball with properties from the 16th and 17th centuries. The effect of impulsive loading on the material properties was accounted for using existing dynamic increase factors. The problem was solved using the explicit dynamic analysis available in Abaqus/Explicit. The different modelling strategies were compared and discussions on the use of different approaches were raised.

**Keywords:** Rammed earth · Finite element modelling · Impact analysis · Dynamic increase factors

## 1 Introduction

Impact loading analysis plays an important role in structural engineering, both within the modern-day context and historical contexts. Depending on the type of impactor itself, the structure may exhibit either a local response, such as a dent/hole in a section, or a global response, such as a progressive collapse. In this paper, a portion of the *Torre de la Vela*, a tower in the Alhambra in Grenada, Spain, was studied under impact loading using Finite Element Methods (FEM). The local response of the building in the region of impact of a historical cannon ball and a hypothetical impactor was investigated. Models using continuum elements with and without the removal of damaged elements, and a model using contact elements were compared to assess the damage from the impactor.


Y. Endo and T. Hanazato (Eds.): SAHC 2023, RILEM Bookseries 46, pp. 143–155, 2024.
https://doi.org/10.1007/978-3-031-39450-8_12

## 2 Materials and Models

Impact loading is categorized as an "impulsive load". Upon impact of an object on a structure, the structural response will depend on the velocity and the material properties of the object in motion, and of the structure itself. Consequently, if a minor object hits a structure at a high velocity, local damage around the impact zone will develop faster than the global deformation of the structure being struck. Furthermore, the stresses in both the object and the structure will depend on their respective material properties [1]. Under concentrated loading, the structural component can demonstrate both a local and a global failure response (Fig. 1).

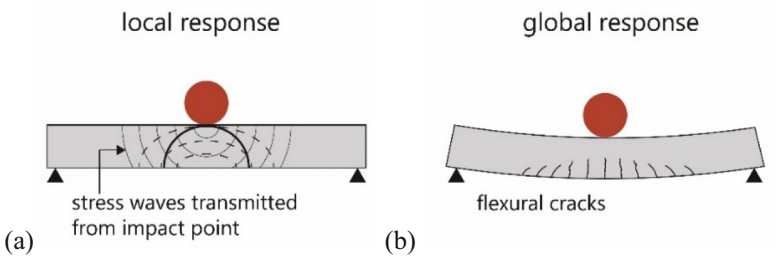


**Fig. 1.** Concrete beams subjected to impact loading: (a) local response; (b) global response (adapted from [2]).

Impact loads can be classified either by their intensity and duration, or by the dissipative mechanism.

– *Intensity and Duration.* Loads classified by intensity and duration can be further classified in three sub-categories: particle impact, rigid body impact, and transverse impact on flexible bodies [3].

- *Particle Impact* is an analytical approximation where only the normal component of the impact force is taken into consideration. This type of classification is for large forces of negligible duration; it provides a simple solution when only the impacts of kinematics are considered, and the structural vibration is negligible.
- *Rigid Body Impact* is the classification used when the contact area between two compact bodies is small relative to its overall dimensions. The stress created in the contact area decreases significantly as the radial distance from the contact region increases. Various contact laws can be used to obtain the time-history of the impact force. This classification of impact can be modelled using the massive beam and the effective mass models.
- Transverse impact on flexible bodies occurs when one of the bodies displaces in bending from the impact force, resulting in a lower impact force from the reduction in stiffness.

– *Dissipative Mechanism.* Loads classified by their dissipative mechanism can be classified in two ways: soft impact and hard impact [4].

- *Soft impact mechanisms* occur between two rigid bodies. Here, most of the kinetic energy is dissipated by the impacted structure.
- *Hard impact mechanisms* occur between two objects with deformable components. In this mechanism, the initial kinetic energy is dissipated by the impactor.

Two simplified approaches can be used to understand the structural response of a subject to soft and hard impacts [4]. A single degree of freedom problem can be used to understand the global effect of soft impacts (Fig. 2a), whereas a two degree-of-freedom problem is used for hard impacts (Fig. 2b). In the soft impact model, a distributed impact load, $p(t)$, acts on the partial mass of the structure, $M_1$. The impact load can then be idealized with a point-mass connected to a spring element, representing the global stiffness of the member under an equal concentrated dynamic load. In the hard impact model, the impactor is modelled as a mass and not as a distributed load. The idealized system is then represented as two lumped masses, $M_1$ and $M_2$, connected by a spring.

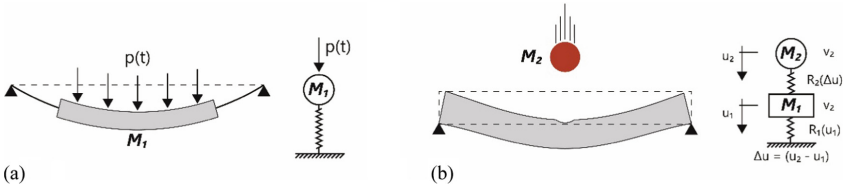


**Fig. 2.** Simplified models recommended by Eurocode for structures under impact loads (adapted from [4]).

Numerical simulation can be used to analyze structures under impact loading. Materials subjected to different impact speeds will have different strength properties, which in turn modifies the material's resistance to penetration. Methods of identification can be used to describe the material properties of a structure subjected to impactors at different velocities. Amongst the material models available, those often used for numerical modelling of solid penetration through the structure include: the Mohr-Coulomb model, the Johnson-Cook mode, the Zerilli-Armstrong model, and the thermos-mechanical material model [5].

Impact loads can produce very high strain rates in the range of $10^0$ to $10^2$ $s^{-1}$, which alters the dynamic mechanical properties of the structure being impacted [6]. As the dynamic mechanical properties are greater in strength than the static properties, dynamic increase factors (DIFs) can be used to account for the difference in properties. The DIFs for Young's Modulus, $E$, and the compressive strength of rammed earth were calculated using a strain rate of 100 $s^{-1}$ using equations determined in previous work by Pereira [7]. As the DIFs for tensile strength of the rammed earth was unavailable, these DIFs were assumed to be the same as the compressive strength. The DIFs used in this research can be seen in Table 1, and the material properties with and without accounting

for the dynamic increase factors can be seen in Table 2, in line with previous work by the authors [8].

**Table 1.** Dynamic increase factors for the brick masonry under impact loading.

| Material Property | DIF (Rammed Earth) |
|---|---|
| $E$ | 2.65 |
| $\sigma_c$ | 1.76 |
| $\sigma_t$ | 1.76 |

**Table 2.** Material properties for rammed earth in the *Torre de la Vela*, before and after being updated using the DIFs.

| Material Property | Original Value | Value with DIF |
|---|---|---|
| $\boldsymbol{E}$ [kN/m$^2$] | $1.60 \times 10^6$ | $4.25 \times 10^6$ |
| $\boldsymbol{\nu}$ [−] | 0.25 | 0.25 |
| $\boldsymbol{\rho}$ [T/m$^3$] | 1.60 | 1.60 |
| $\boldsymbol{\sigma_c}$ [kN/m$^2$] | 4000 | 7020 |
| $\boldsymbol{G_{fc}}$ [kN/m] | 6.40 | 11.24 |
| $\boldsymbol{\sigma_t}$ [kN/m$^2$] | 200 | 351 |
| $\boldsymbol{G_{ft}}$ [kN/m] | 0.013 | 0.019 |

Ballistic impact can be simulated using Abaqus/Explicit. The explicit dynamic analysis procedure in Abaqus/Explicit implements an explicit integration rule combined with diagonal or "lumped" element matrices [5]. The calculation of the nodal accelerations at any point in time, $\ddot{\boldsymbol{u}}(t)$, can be calculated using the lumped mass matrix, $\boldsymbol{M}$, the internal and external forces, $\boldsymbol{F}(t)^{int}$ and $\boldsymbol{F}(t)^{ext}$, respectively, using Eq. 1.

$$\ddot{\boldsymbol{u}}(t) = \boldsymbol{M}^{-1} \bullet \boldsymbol{F}(t)^{ext} - \boldsymbol{F}(t)^{int} \tag{1}$$

Masonry structures can be numerically represented using several approaches, including macro-modelling, detailed micro-modelling, and simplified micro-modeling [9]. In the simplified facade model of the *Torre de la Vela*, a combination of macro-modeling and simplified micro-modeling approaches were used.

Previous authors have used to Concrete Damaged Plasticity (CDP) model for masonry buildings under high strain rates from blast loading [10, 11], concrete members subjected to high strain rates [12], and rammed earth constructions under seismic events [13]. The CDP model, a modification of the Drucker-Prager model [14, 15], was the constitutive model adopted in Abaqus for this work. The CDP material model uses the concepts of isotropic damage evolution, and isotropic tensile and compressive plasticity to represent the behaviour of the material in the inelastic or fracture ranges. This model

also allows the strain softening in tension and strain hardening in compression to be defined, as it assumes that damage plasticity characterizes the failure in tension and compression.

The values for the dilation angle, flow potential eccentricity, ratio of initial equibiaxial compressive yield stress to the initial uniaxial compressive yield stress, and viscosity parameter were defined according to work by Mohamad and Chen [16]. The parabolic stress-strain law and the exponential stress-strain law were selected for the compressive and tensile behaviour of the rammed earth, respectively. A damage parameter of 0.95 was assigned to the maximum tensile strain of the rammed earth as the damage criterion.

For the micro-modelling approach, the Mohr-Coulomb model was selected to represent the sliding failure of the frictional interfaces between the contact elements. The model assumes non-associative flow and the dilatancy angle in the model was assigned a value of zero, as this interaction does not work within the plasticity framework [17, 18]. The use of a dilation angle of zero produces more conservative results, since the strength of the material increases with the dilation angle [19]. Since the Mohr-Coulomb failure criterion cannot be modeled in Abaqus, the cohesion was considered as negligible in this analysis. The normal and tangent stiffness of the rammed earth blocks were based on previous literature [17]. When modelling contact elements (or discrete elements), the joint stiffness must be taken into consideration to ensure the same wall stiffness as with continuum elements. As such, the Young's Modulus of the contact elements could be recalculated based on Lourenço et al. to account for the joint stiffness [20]. The friction coefficient was taken as the average value from literature [17, 21–23]. A summary of the interaction properties used for the micro-modelling approach can be seen in Table 3.

**Table 3.** Interaction properties

| Normal Stiffness, $K_{n,joint}$ | Tangent Stiffness, $K_{s,joint}$ | Young's Modulus (Contact Elements) | Friction Coefficient |
|---|---|---|---|
| $1.50 \times 10^8$ kN/m$^3$ | $7.50 \times 10^7$ kN/m$^3$ | $1.12 \times 10^9$ kN/m$^2$ | 0.73 |

The use of the "removal of damaged elements" feature in Abaqus allows to better understand the failure occurring when a model is subjected high levels of damage [24]. Using this feature, elements which reach a maximum level of degradation are removed from the model during analysis. In Abaqus/Explicit, this occurs when the maximum degradation point occurs at a single integration point in the element. The advantage of using this feature is that highly distorted elements are removed from the analysis. However, in case of substantial damage, the accuracy of simulation will decrease as the deletion of damaged elements also removes mass and energy from the system.

## 3 Impact Loading on the *Torre de la Vela*

The first known examples of cannons date from the Song dynasty in China, around the 12th century [25]. Evidence of cannons in the Middle East appeared in the 14th century, and cannons were used soon after in Europe. By the end of the 14th century,

cannons were widespread in Europe [26]. Cannons were particularly important during the Grenada War, fought between the Catholic Monarchs and the Nasrid Dynasty's Emirate of Granada. The diameter, weight, and velocities of the impactor in this work was selected based on the properties of 17th century Spanish cannons [27–30].

Two loading scenarios were studied in this analysis, corresponding to a 16th century cannon ball, and a larger hypothetical cannon ball. The properties of both impactors can be seen in Table 4. The fourth floor of the Torre de la Vela was selected as the location of the impact. As the size of the impactors were negligible compared to the size of the walls, a local response was expected and only the upper portion of the tower was modelled.

**Table 4.** Properties of the historical and hypothetical impactors.

| | Diameter | Density | Velocity | Young's Modulus | Poisson's ratio |
|---|---|---|---|---|---|
| Historical | 13 cm | 6.31 T/m$^3$ | 408 m/s$^2$ | 165 $\times$ 10$^6$ kN/m$^2$ | 0.27 |
| Hypothetical | 50 cm | 6.31 T/m$^3$ | 600 m/s$^2$ | 165 $\times$ 10$^6$ kN/m$^2$ | 0.27 |

### 3.1 Effects of 16$^{th}$ Century Cannonballs

Three different models were created to assess the effect of 16$^{th}$ century cannonballs on the *Torre de la Vela*: a continuum model with the removal of damaged elements, a continuum model without the removal of damaged elements (Fig. 3a), and a contact model (Fig. 3b). General purpose tetrahedron pyramid elements (C3D10) were used, with varying mesh sizes such that a finer mesh was used around the location of impact. The cannon ball was modelled as a soft-body impactor, at an initial distance of 0.02 m from the wall which reduced the computational time of the analysis (Fig. 3c). The interaction between the impactor and the structure wall was defined by general contact. Hard contact was used as the normal behaviour of the contact property, with separation allowed after contact. In the continuum element model, the mesh was refined around the impact location.

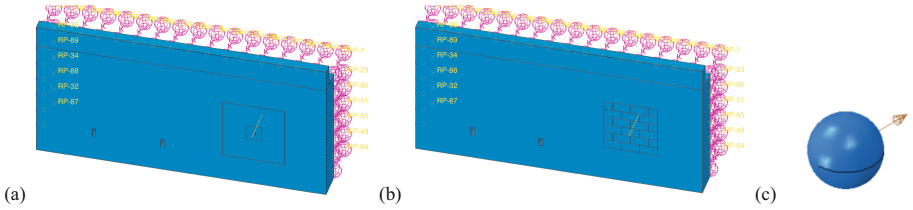


(a) (b) (c)

**Fig. 3.** Loading definition: (a) continuum model; (b) contact element model; (c) impactor.

Negligible damage occurred in both the continuum models with and without the removal of damaged elements, and the stress distributions for both continuum models were identical. Consequently, the results from the continuum model with removable damaged elements will not be presented. The time history of the compressive stresses

in the wall at and after impact can be seen in Fig. 4, with the time normalized such that the impact occurs at 0.0 s. The lower bound of the compressive stress is plotted at 100 kN/m$^2$, which is significantly lower than the actual compressive strength of the rammed earth of 4390 kN/m$^2$. The contact model dissipates energy faster than in the continuum model, as there is a higher concentration of compression stresses found at the location of impact in the continuum model but not in the contact model at 0.006 s (Fig. 4). In the contact element model, the compressive stresses are mostly confined to the contact block when the projectile impacts the wall. As the energy dissipates, the contact block impacted applies compressive stresses on the blocks horizontally adjacent to the initial block. Additionally, the stresses in the continuum model are transferred from the front to the back of the wall, which does not occur in the contact element model (Fig. 5).

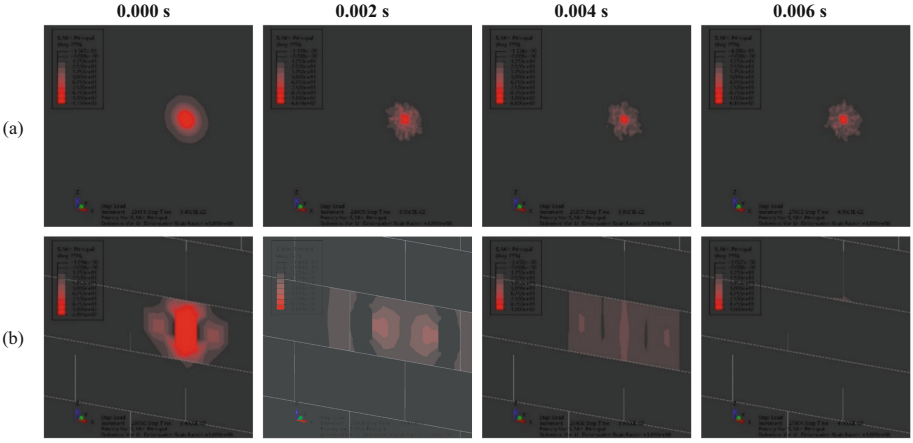


**Fig. 4.** Time history of compression stresses immediately after impact on the front of the wall: (a) continuum model; (b) contact model

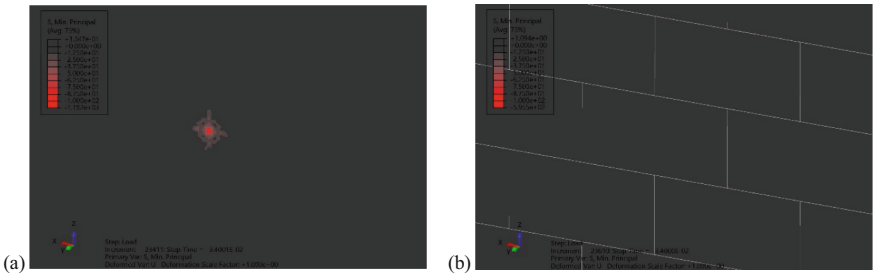


**Fig. 5.** Compression stresses in the back of the models after impact: (a) continuum model; (b) contact element model.

The time history of the tensile stresses in the wall at and after impact can be seen in Fig. 6, with the time normalized to the impact occurring at 0.0 s. The upper bound of the tensile stresses is plotted at 100 kN/m$^2$, which is significantly lower than the tensile

strength of the rammed earth of 527 kN/m$^2$. At the moment of impact, the tensile stresses are much lower in the continuum model than in the contact model. No tensile stresses are present where the impact strikes the wall in the contact model, which is likely due to the compressive stresses at that location. Nonetheless, there is still a large concentration of tensile stresses at the location of impact in the continuum model, likely caused by the extrapolation of the tensile stresses to the nodes in that region. The tensile stresses dissipate much faster in the contact model than in the continuum model, which is similar to the previously mentioned compressive stresses. The distribution of the tensile stresses in both the continuum and the contact models differ as well. In the continuum model, the tensile stress is concentrated at the point of impact and expands radially from its center. In the contact model, only the element struck by impact have tensile stresses, with those stresses being confined to that block element in both horizontal and vertical directions. As with the compressive stresses, a tensile stress concentration is visible at the back of the wall for the continuum model, but not in the contact model.

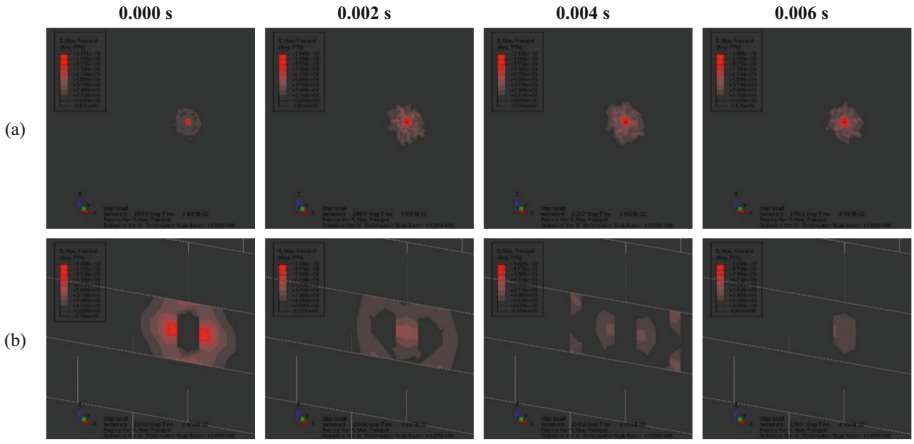


**Fig. 6.** Time history of tensile stresses immediately after impact on the front of the wall: (a) continuum model; (b) contact model.

### 3.2 Effects of a Hypothetical Impactor

Since the 16$^{th}$ century cannonball did not cause any damage to the model, a hypothetical impactor was modelled to analyse the effect of impact loading using the removal of damaged elements feature in Abaqus. The diameter and initial velocity of the cannonball were updated for this analysis (see Table 4), but the remaining properties of the impactor and the continuum model remain the same.

Minor damage to the surface of the wall was observed, characterized by the removed elements at the surface of the model (Fig. 7). As with the previous impactor, the lower bound of the compressive stress is plotted at 100 kN/m$^2$, which is significantly lower than the compressive stress of the rammed earth of 4390 kN/m$^2$. The damage in the wall

increases significantly between 0.0 s and 0.4 s, but the change in damage is minimal between 0.4 s and 0.6 s. Likewise, the stress distribution at the location of impact does not change significantly between 0.4 s and 0.6 s. The stress distribution in the wall is localized in the area surrounding the damage caused by the impactor. The higher values of compressive stress are located inside the hole caused by the impactor, with little stress at the perimeter of the hole. Although several elements have been removed, the compressive stresses in the wall are still well below the compressive strength of the rammed earth masonry for the remaining elements.

As with the compressive stresses, the tensile stresses are mostly located around the damaged area of the wall (Fig. 8). In Fig. 8, the upper bound of the tensile stresses is plotted at 200 kN/m$^2$, which is lower than the tensile strength of the rammed earth of 527 kN/m$^2$. The higher values of tensile stress are in the regions surrounding the hole caused by the impactor, but not inside the hole itself.

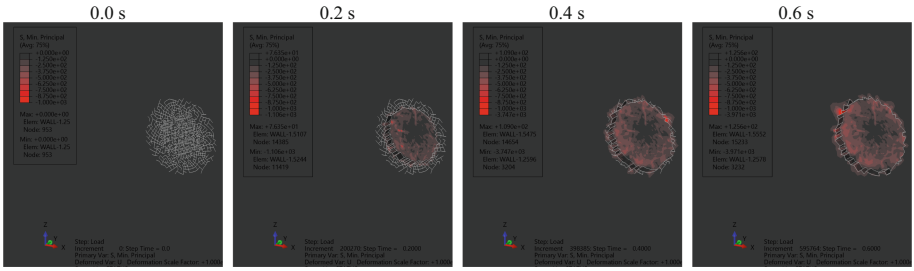


**Fig. 7.** Time history of compression stresses in the wall caused by the hypothetical impactor.

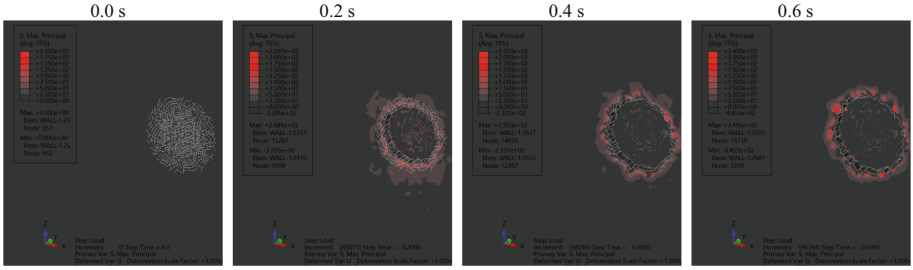


**Fig. 8.** Time history of tensile stresses in the wall caused by the hypothetical impactor.

## 4 Discussion

When looking at the results from the 16th-century cannonball, both models show similar displacement trends after impact, as seen in the plot of the displacement at the impacted node over time (Fig. 9a). Through the displacement from the continuum model is greater than the contact model, both displacements can be considered as negligible. This difference in displacement is likely caused by a difference in energy that remains in the system after the impact (Fig. 9b). After impact, the energy in the continuum model remains constant, whereas the energy in the contact model increases and decreases sharply before remaining constant.

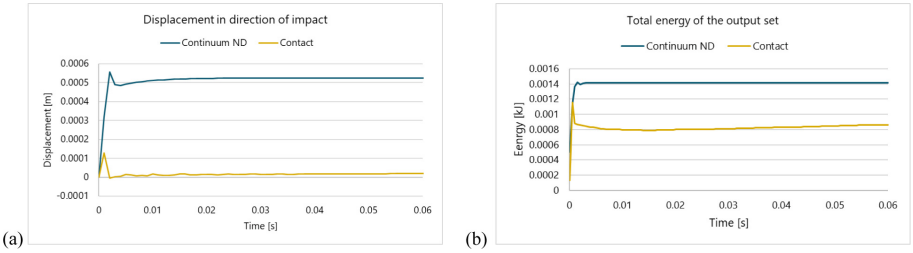


**Fig. 9.** (a) Displacement at the impacted node in the direction of the load; (b) total energy of the output set.

The diameter of hole caused by the impactor over time followed a logarithmic trend (Fig. 10). At the end of the analysis, the diameter of the hole remained constant, with a maximum diameter of 53 cm. This maximum diameter is slightly larger than the diameter of the impactor (50 cm), indicating the maximum size of the possible damage is approximately the same size as the impactor. The depth of the hole caused by the impactor was approximately 6.2 cm and was constant over the depth damaged area. An inspection of the mesh showed that the depth of the damage corresponds to the depth of a single layers of elements in that location. Since the damaged elements in Abaqus are removed when a single integration point in the element reaches the damage threshold, the depth of the damage caused by the impactor is mesh dependent. Consequently, the mesh would need to be refined further in the area of the impact to understand the true effects of the hole caused by an impactor.

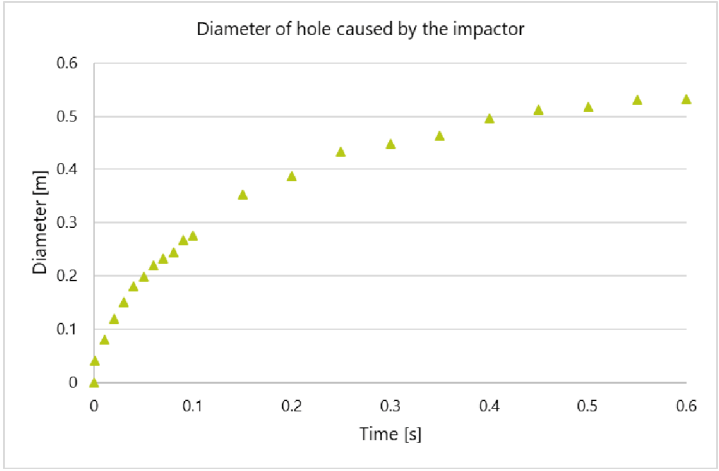


**Fig. 10.** Time history of the diameter of the hole caused by the hypothetical spherical impactor.

## 5 Conclusions

When assessing the effect of a 16th century cannonball on a wall in the *Torre de la Vela*, three models of a wall section of the tower were created: a continuum model, a continuum model with removal of damaged elements, and a contact model. In all three models, the 16th century cannonball would not cause any damage to the *Torre de la Vela*. Some differences in displacement occurred between the continuum model and the contact element model, as a result of the energy dissipation in the structure following impact. A hypothetical spherical impactor was modelled to better understand the damage caused by an impactor in the continuum model. This second impactor caused localized damage on the surface of the wall, where the diameter of damage was slightly larger than the diameter of the impactor. The depth of the damage also corresponded to the size of the mesh elements in the region of impact. Future work should consider the use of a more refined mesh in the region of impact to better replicate the potential damage of an impactor on the surface of the rammed earth masonry walls.

## References

1. Ekström, J.: Blast and Impact Loaded Concrete Structures: Numerical and Experimental Methodologies for Reinforced Plain and Fibre Concrete Structures. Chalmers University of Technology, Gothenburg (2017)
2. Fujikake, K., Li, B., Soeun, S.: Impact response of reinforced concrete beam and its analytical evaluation. J. Struct. Eng. **135**(8), 938–950 (2009). https://doi.org/10.1061/(ASCE)ST.1943-541X.0000039
3. Kam-wing Wong, J.: Structures under Impact Loading," Bachelor Thesis, University of Cambridge, Cambridge (2005)
4. CEN, Eurocode 1: Actions on Structures. Brussels: European Committee for Standardization (2003)

5. Žmindák, M., Pelagić, Z., Pastorek, P., Močilan, M., Vyboštok, M.: Finite Element modelling of high velocity impact on plate structures. Procedia Eng. **136**, 162–168 (2016). https://doi.org/10.1016/j.proeng.2016.01.191
6. Ngo, T., Mendis, P., Gupta, A., Ramsay, J.: Blast loading and blast effects on structures – an overview. Electron. J. Struct. Eng. **7**, no. Special Issue: Loading on Structures, pp. 76–91 (2007)
7. Pereira, J.M., Lourenço, P.B.: Experimental characterization of masonry and masonry components at high strain rates. J. Mater. Civ. Eng. **29**(2), 04016223 (2017). https://doi.org/10.1061/(ASCE)MT.1943-5533.0001755
8. Tse, D., Pereira, J.M., Lourenço, P.B.: Numerical analysis of an earthen masonry structure subjected to blast loading. CivilEng **2**(4), 969–985 (2021). https://doi.org/10.3390/civileng2040052
9. P. B. Lourenço, "Structural masonry analysis: recent developments and prospects," presented at the Proc. of the 14th International Brick/Block Masonry Conference, Australia, 2008
10. Pereira, J.M., Lourenço, P.B.: Risk assessment due to terrorist actions on public transportation networks: a case study in Portugal. Int. J. Prot. Struct. **5**(4), 391–415 (2014)
11. Pereira, J.M., Campos, J., Lourenço, P.B.: Masonry infill walls under blast loading using confined underwater blast wave generators (WBWG). Eng. Struct. **92**, 69–83 (2015). https://doi.org/10.1016/j.engstruct.2015.02.036
12. Altaee, M., Kadhim, M., Altayee, S., Adheem, A.: Employment of damage plasticity constitutive model for concrete members subjected to high strain-rate. In: Proceedings of the 1st International Multi-Disciplinary Conference Theme: Sustainable Development and Smart Planning, IMDC-SDSP 2020, Cyperspace, 28–30 June 2020, Cyberspace, 2020. https://doi.org/10.4108/eai.28-6-2020.2298164
13. Bui, Q.-B., Bui, T.-T., Tran, M.-P., Bui, T.-L., Le, H.-A.: Assessing the seismic behavior of rammed earth walls with an L-form cross-section. Sustainability **11**(5), 1296 (2019). https://doi.org/10.3390/su11051296
14. Lee, J., Fenves, G.L.: Plastic-damage model for cyclic loading of concrete structures. J. Eng. Mech. **124**(8), 892–900 (1998). https://doi.org/10.1061/(ASCE)0733-9399(1998)124:8(892)
15. Lubliner, J., Oliver, J., Oller, S., Oñate, E.: A plastic-damage model for concrete. Int. J. Solids Struct. **25**(3), 299–326 (1989). https://doi.org/10.1016/0020-7683(89)90050-4
16. Abdelmoneim Elamin Mohamad, A.-B., Chen, Z.: Experimental and numerical analysis of the compressive and shear behavior for a new type of self-insulating concrete masonry system. Appl. Sci. **6**9, 245 (2016). https://doi.org/10.3390/app6090245
17. Shrestha, K.C., Aoki, T., Miyamoto, M., Wangmo, P., Pema: In-Plane shear resistance between the rammed earth blocks with simple interventions: experimentation and finite element study. Buildings **10**(3), 57 (2020). https://doi.org/10.3390/buildings10030057
18. Lourenço, P.B., Ramos, L.F.: Characterization of cyclic behavior of dry masonry joints. J. Struct. Eng. **130**(5), 779–786 (2004). https://doi.org/10.1061/(ASCE)0733-9445(2004)130:5(779)
19. Godio, M., Stefanou, I., Sab, K.: Effects of the dilatancy of joints and of the size of the building blocks on the mechanical behavior of masonry structures. Meccanica **53**(7), 1629–1643 (2017). https://doi.org/10.1007/s11012-017-0688-z
20. Lourenço, P.B., Oliveira, D.V., Roca, P., Orduña, A.: Dry joint stone masonry walls subjected to in-plane combined loading. J. Struct. Eng. **131**(11), 1665–1673 (2005). https://doi.org/10.1061/(ASCE)0733-9445(2005)131:11(1665)
21. Bui, T.-L., Bui, T.-T., Bui, Q.-B., Nguyen, X.-H., Limam, A.: Out-of-plane behavior of rammed earth walls under seismic loading: Finite element simulation. Structures **24**, 191–208 (2020). https://doi.org/10.1016/j.istruc.2020.01.009

22. Wangmo, P., Shrestha, K.C., Miyamoto, M., Aoki, T.: Assessment of out-of-plane behavior of rammed earth walls by pull-down tests. Int. J. Archit. Herit. **13**(2), 273–287 (2019). https://doi.org/10.1080/15583058.2018.1433903
23. El-Nabouch, R., Bui, Q.-B., Plé, O., Perrotin, P.: Characterizing the shear parameters of rammed earth material by using a full-scale direct shear box. Constr. Build. Mater. **171**, 414–420 (2018). https://doi.org/10.1016/j.conbuildmat.2018.03.142
24. ABAQUS, ABAQUS User's Manual, vol. Version 2019. Waltham, MA: Dassault Systèmes (2010)
25. Gwei-Djen, L., Needham, J., Chi-Hsing, P.: The oldest representation of a bombard. Technol. Cult. **29**(3), 594 (1988). https://doi.org/10.2307/3105275
26. Andrade, T.: The Gunpowder Age: China, Military Innovation, and the Rise of the West In World History. Princeton University Press, Princeton Oxford (2016)
27. Manucy, A.C.: Artillery Through the Ages. United States Department of the Interior, Washington (1949)
28. Hall, A.R.: Ballistics in the Seventeenth Century: A Study in the Relations of Science and war with Reference Principally to England, First published 1952, Digitally printed version 2009. University Press, Cambridge (1952)
29. "Cannon," Wikipedia. May 09, 2021. [Online]. https://en.wikipedia.org/wiki/Cannon
30. "What Sank the Armada?," Battlefield Detectives, Discovery Chanel, USA, Oct. 25 (2004)